american physiological society

JNP JOURNAL OF NEUROPHYSIOLOGY

J Neurophysiol 133: 85–100, 2025.
First published November 19, 2024; doi:10.1152/jn.00368.2024

RESEARCH ARTICLE

Sensory Processing

Perisaccadic perceptual mislocalization strength depends on the visual appearance of saccade targets

Matthias P. Baumann,[1,2]* Anna F. Denninger,[1,2,3,4]* and Ziad M. Hafed[1,2]

[1]*Werner Reichardt Centre for Integrative Neuroscience, University of Tübingen, Tübingen, Germany;* [2]*Hertie Institute for Clinical Brain Research, University of Tübingen, Tübingen, Germany;* [3]*Department for Psychiatry and Psychotherapy, University of Tübingen, Tübingen, Germany; and* [4]*Center for Mental Health (TüCMH), University of Tübingen, Tübingen, Germany*

Abstract

We normally perceive a stable visual environment despite eye movements. To achieve such stability, visual processing integrates information across a given saccade, and laboratory hallmarks of such integration are robustly observed by presenting brief perisaccadic visual probes. In one classic phenomenon, probe locations are grossly mislocalized. This mislocalization is believed to depend, at least in part, on corollary discharge associated with saccade-related neuronal movement commands. However, we recently found that superior colliculus motor bursts, a known source of corollary discharge, can be different for different image appearances of the saccade target. Therefore, here we investigated whether perisaccadic mislocalization also depends on saccade target appearance. We asked human participants to generate saccades to either low (0.5 cycles/°) or high (5 cycles/°) spatial frequency gratings. We always placed a high-contrast target spot at grating center, to ensure matched saccades across image types. We presented a single, brief perisaccadic probe, which was high in contrast to avoid saccadic suppression, and the subjects pointed (via mouse cursor) at the seen probe location. We observed stronger perisaccadic mislocalization for low-spatial frequency saccade targets and for upper visual field probe locations. This was despite matched saccade metrics and kinematics across conditions, and it was also despite matched probe visibility for the different saccade target images (low vs. high spatial frequency). Assuming that perisaccadic visual mislocalization depends on corollary discharge, our results suggest that such discharge might relay more than just spatial saccade vectors to the visual system; saccade target visual features can also be transmitted.

NEW & NOTEWORTHY Brief visual probes are grossly mislocalized when presented in the temporal vicinity of saccades. Although the mechanisms of such mislocalization are still under investigation, one component of them could derive from corollary discharge signals associated with saccade movement commands. Here, we were motivated by the observation that superior colliculus movement bursts, one source of corollary discharge, vary with saccade target image appearance. If so, then perisaccadic mislocalization should also do so, which we confirmed.

corollary discharge; perisaccadic mislocalization; saccadic compression; spatial frequency; superior colliculus

INTRODUCTION

Vision is a highly active process, continuously utilizing eye movements to both sample and modulate incoming retinal image streams. Because eye movements, such as saccades, necessarily shift retinal images even with a completely stable environment, perceptual processes bridging inter- and intrasaccadic image sequences are supposed to take place (1–4). One classic approach to the study of perisaccadic vision has been to present very brief visual probes before, during, and after saccades (5–11). Such presentation has led to two classic observations. First, there is a strong reduction in visual sensitivity to brief perisaccadic probes (7–9, 12–14), called perceptual saccadic suppression. Second,

*M. P. Baumann and A. F. Denninger contributed equally to this work.
Correspondence: Z. M. Hafed (ziad.m.hafed@cin.uni-tuebingen.de).
Submitted 20 August 2024 / Revised 6 November 2024 / Accepted 11 November 2024

with high-contrast probes, these probes are successfully detected but grossly mislocalized relative to their true displayed positions (5, 6, 10, 11, 15–18), in a phenomenon called perisaccadic mislocalization.

Perisaccadic mislocalization has different properties depending on the visual and motor conditions under which it is observed. For example, the presence of visual reference frames makes the mislocalization appear like a convergence toward the saccade target (15). That is, brief probes presented ahead of the saccade target are mislocalized backward in position, and probes presented nearer to the initial fixation position than the saccade target are reported as being forward in position (11). On the other hand, mislocalization is uniform in direction in complete darkness (5, 6, 15), meaning that both probes ahead of and nearer to the initial fixation point than the saccade target are mislocalized in a forward direction parallel to the saccade vector. In addition, with the convergent mislocalization (which we focus on here), the two-dimensional landscape of perisaccadic mislocalization strongly depends on saccade direction, with upward saccades causing particularly large backward errors for probes presented ahead of the saccade target (17).

Because the properties of perisaccadic mislocalization depend on the visual conditions, one neuronal mechanism underlying this phenomenon could be sensory in nature (19). For example, in some models, classic perisaccadic convergent mislocalization (11) can be easily explained using saccade-induced retinotopic shifts of probe representations from the periphery to the perifovea; when these shifts occur on anatomically distorted topographic visual maps having foveal magnification, then a so-called "compression" is a simple consequence of readout from such anatomically distorted maps (20). Indeed, a simple modification of such models to include both foveal as well as upper visual field magnification can also conceptually account for the greater mislocalization strength observed for upward saccades (17). Specifically, in a sensory-motor area such as the superior colliculus (SC), there exist both foveal (21) as well as upper visual field (22) magnification. Thus, if mislocalization depends on how retinotopic representations of probes are translated from the periphery to the fovea on anatomically distorted maps, then larger perisaccadic mislocalization for upward saccades would be expected if such maps additionally differentially represent the upper visual field (17).

Having said that, it is also generally assumed that perisaccadic mislocalization does have a motor component associated with it. Besides the different representations for upward saccades in the SC (22, 23), and the resultant implications for mislocalization strength (17), the SC is a known source of saccade-related corollary discharge signals (24–31). Such corollary discharge signals are sufficient to cause perisaccadic retinotopic remapping of visual response fields in the cortex (32). Thus, if such cortical remapping is indeed one neuronal basis for perceptual mislocalization (33, 34), despite some controversy (35–38), then studying the roles of SC saccade-related discharge in perceptual mislocalization is very worthwhile.

One interesting recently reported property of SC motor discharge is related to the saccade target's visual appearance. Specifically, we recently observed that SC motor bursts can be different for different saccade target images, even under matched saccade metrics and kinematics (39). Since SC motor bursts are relayed to the cortex virtually unchanged (25), this implies that perisaccadic corollary discharge from the SC (24, 26, 32) may potentially relay not only the movement vector information to the cortex but also integrated information about the visual appearance of the saccade target. If so, then perceptual phenomena that are believed to depend, at least partially, on perisaccadic corollary discharge, such as perisaccadic mislocalization, may be additionally modulated by the visual appearance of the saccade target. This is what we investigated here.

METHODS

Experimental Subjects and Ethical Approvals

We ran a visual mislocalization paradigm on eight human subjects (4 female), aged 23–29 yr. We also ran a control experiment testing the detectability of perisaccadic visual probes on eight human subjects (5 female), aged 23–27 yr. Four subjects were shared between the two paradigms, performing both variants of the experiments in different sessions.

The experiments were approved by ethical committees at the Medical Faculty of the University of Tübingen, and the subjects provided written informed consent. They were also financially compensated for their time, and the experiments were in line with the Declaration of Helsinki.

Laboratory Setup

The laboratory setup was the same as that used in our recent studies (14, 40), and we largely used similar procedures. Briefly, the subjects sat in a dark room 57 cm from a calibrated and linearized CRT display with 41 pixels/° resolution. We tracked their eye movements at 1 kHz with a desk-mounted video-based eye tracker (EyeLink 1000; SR Research), and we stabilized their head position with a custom-built apparatus described previously (41). Stimuli were presented on a gray background of 20.01 cd/m^2 luminance, and fixation spots (7 × 7 min arc) were white (with 49.25 cd/m^2 luminance). The experiments were controlled with the Psychophysics Toolbox (42–44) with EyeLink Toolbox extensions (45).

Experimental Procedures

Perisaccadic mislocalization experiment.

In the perisaccadic mislocalization experiment, the subjects fixated a white spot placed ∼8.5° either to the right or left of display center. After 500 ms, a low [0.5 cycles/° (cpd)] or high (5 cpd) spatial frequency Gabor grating was presented at screen center. The grating had a Gaussian smoothing window with $\sigma = 0.49°$ (and thus spanned a diameter of ∼2.4°), and it had high contrast (100%); its phase was also randomized. The subjects were still required to maintain fixation for another 1,000–1,500 ms (because we wanted to avoid any sensory transients associated with grating onset). When the fixation spot was removed, the subjects made a saccade toward the center of the grating, which had a central marker in its middle as in our neurophysiology experiments (39) (to minimize intertrial saccade variance and to also control for postsaccadic fixation position). This instructed, visually

guided saccade was the one of primary experimental interest for us in this study, because it was only this saccade that we paired with a strategically timed visual probe for localization. Specifically, once we detected a saccade onset after fixation spot removal, we presented a brief (1 frame; 85 Hz refresh rate in the display) flash of a white square (that is, of high contrast) of size 45 × 45 min arc (Fig. 1A). The times of the flash were either immediately upon online saccade detection or at +40 or +80 ms from such detection. In post hoc analyses, we recomputed the flash times to always report them relative to actual saccade onset (see *Data Analysis* and RESULTS).

Our online saccade detection algorithm was the same as the one that we used previously (14, 40, 46, 47). Briefly, we obtained a real-time estimate of radial eye speed by having a running history of recent eye position samples and how these samples differed (locally in time) from each other. Specifically, at every time sample, we obtained a best-fitting line to the latest five measurements of eye position data that were collected. We then took the slope of the fitted line as an indication of the rate of change in eye position. To reduce noise, we took the median of the three latest slope measurements as our final estimate. That is, at the current time t ms, we took the slope of the line best fitting the eye positions collected between times $t - 4$ ms and t ms. We then combined it with the slope calculated from the previous time sample (measuring eye positions from $t - 5$ ms to $t - 1$ ms) and the sample before that (measuring eye positions from $t - 6$ ms to $t - 2$ ms). The median of these three latest slope calculations was considered our rate of change of eye position, and we applied a user-adjustable threshold to decide whether this rate of change was large enough to qualify as a saccade onset. The key was to pick a threshold above the current noise levels of the eye tracker, and our use of the median helped stabilize our estimates against noise (with the small expense of needing to buffer up to time sample $t - 6$ ms for the calculations).

The behavioral task of the subjects was to indicate (with a computer mouse cursor) the perceived location of the recently presented flash. Specifically, after the subjects fixated the central grating for 500 ms (that is, after the end of the primary saccade), we removed all stimuli from the display and displayed a mouse cursor at display center. The subjects clicked on the seen flash location, and they were free to move their eyes until they responded (they typically made secondary saccades toward where they reported the flash position with the mouse cursor; see RESULTS). The mouse cursor itself was the standard cursor of the Mac OS operating system through which we controlled the experimental display: it was a black, oblique arrow spanning a total of ~14.4 min arc horizontally and 19.2 min arc vertically. It was thus significantly smaller than the perisaccadic flash, especially since the registered click location of the cursor was actually the single-pixel tip of the entire mouse cursor's arrow shape.

The mouse was moved by the subjects on a flat table-top surface orthogonal to the orientation of the vertical visual display in front of the subjects. However, our subjects were all highly experienced in using computers, so there was no learning involved in moving the mouse cursor to its intended position on the display before clicking to register their report. In addition, the mouse cursor was always visible on the display during the entire reporting period, allowing the subjects to accurately click the mouse cursor where they actually intended to do so.

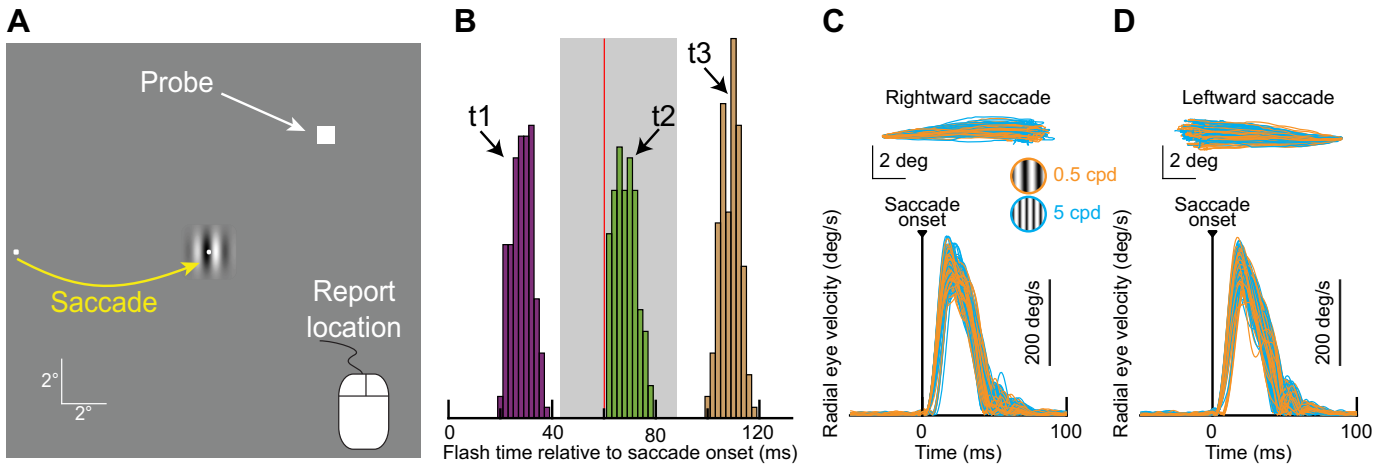

Figure 1. Probing perisaccadic perceptual mislocalization with different saccade target image appearances. *A*: subjects generated a rightward (shown) or leftward saccade toward the center of a low- or high-spatial frequency grating. The center of the grating always had a small spot, to improve saccade accuracy/precision and vector matching across different trials and different saccade target appearances (METHODS). At different times relative to online saccade detection, we presented a very brief probe flash at 1 of 4 positions. Later, all stimuli were removed, and subjects had to point to the perceived flash position with a mouse cursor. Stimuli are drawn to scale (see scale bars). *B*: distribution of probe flash times relative to saccade onset in 1 example subject. We classified flash times according to the 3 seen peaks, and we labeled the categories *t1*, *t2*, and *t3*, respectively. We expected perceptual mislocalization to progressively get smaller and smaller from *t1* to *t3* (11). $N = 460$ trials. The gray region indicates the range of saccade end times observed in this subject, and the red line shows the mean value. *C*, *top*: horizontal and vertical eye position traces for rightward saccades from an example subject. Starting eye positions from all trials were aligned for better visualization of the saccade vectors, and the different colors show saccades toward either the low- or high-spatial frequency grating. *Bottom*: radial eye speed traces from the same trials. Note how saccade metrics (*top*) and kinematics (*bottom*) were matched across image types. Also note how the flash times in *B* spanned intrasaccadic flashes (*t1*) as well as flashes immediately after (*t2*) or later well beyond saccade end (*t3*). $N = 113$ and 117 for low- and high-spatial frequency saccade targets, respectively. cpd, cycles/°. *D*: same as *C* but for leftward saccades from the same subject. $N = 117$ and 113 for low- and high-spatial frequency saccade targets, respectively.

We also did not impose a requirement of speeded responses on the subjects, and this was a deliberate choice to allow them to be as accurate as possible in their reporting of perisaccadic flash location. Thus, we employed a very relaxed maximum duration value of 10 s for every single trial; if there was no subject response when the overall trial length (stimuli plus reaction time) reached 10 s, the computer registered that there was no behavioral response, and the trial was discarded. In reality, the manual reaction times of the subjects were much shorter than 10 s. Across subjects, the mean reaction time (measured 500 ms after the primary saccade, since the removal of the saccade target was the cue to respond in our task) was 996 ± 43 ms (SE), and the median reaction time was 972 ± 41 ms (SE). Moreover, across subjects, the minimum reaction time on any given trial was 466 ± 54 ms (SE), and the maximum reaction time was 2,173 ± 321 ms (SE).

We also note here that our prior work on visual localization (in the absence of perisaccadic visual probe flashes) revealed very minimal reporting errors with memory-based mouse cursor clicks, and this was the case even with several seconds of experimental working memory delay and subsequent reaction times by the subjects (17, 48, 49). Thus, our mislocalization errors reported in RESULTS cannot be explained by memory distortions.

We picked four possible perisaccadic flash locations on the display, each at a radius of ~7.3° from the saccade target center location. One flash was directly opposite the saccade target direction (i.e., on the horizontal axis), and the other three flashes were along the saccade direction and ahead of the saccade target location: one on the horizontal axis directly ahead of the saccade target (along the same vector) and the other two at the ±45° diagonals. Even though the flash opposite the saccade vector was expected to have the least mislocalization (17) (which we confirmed), we included it so that subjects could not expect to always see flashes ahead of the saccade target. Nonetheless, in the analyses (see below), we only analyzed the three flash locations ahead of the saccade target. This is because the mislocalization for the backward flash position was small in amplitude; past work that looked at mislocalization of the flash opposite the saccade vector typically used significantly larger saccades than we used, which made the smaller mislocalization of such a flash easier to detect than in our experiments (11, 16). In addition, and again because of our smaller saccade sizes than in previous studies, this backward probe location was actually close to the initial fixation spot (only ~1° away from it when the eye was still fixated before saccade onset), which made us worry that there could be interactions with the initial fixation spot location in the subjects' reported locations. Thus, it was more appropriate to analyze only the three forward probe flash locations.

Consistent with the above sentiment, we generally wanted to avoid having spatial reference frames (e.g., the edges of the display monitor) strongly influence performance in the visual mislocalization task. Therefore, across trials, we randomly shifted all stimulus positions in a given trial by a random (but constant) number from the range of ±1.2° in either horizontal or vertical direction (at pixel resolution; 1/41°). That is, on every trial, the overall displayed stimulus geometry was randomly shifted on the display monitor from previous trials, so that the monitor edges could not act (across trials) as reliable reference frames for probe flash localization. For example, if the initial fixation position was shifted by 1° to the right of its standard position on a given trial, then the grating position at the center of the display was also shifted by 1° to the right, and so was the perisaccadic probe flash (in other words, the stimulus relationships were all unchanged, but the overall absolute position was shifted by 1° to the right). This approach minimized the possibility of subjects remembering the absolute positions of flashes relative to the display monitor edges across trials. We are thus confident that the results that we report here were less affected by global biases of expected, world-centered, probe flash locations.

Finally, note that the low and high spatial frequencies chosen as the saccade targets were differentially represented by the SC motor bursts in our recent neurophysiological results (39). That is why we chose these particular spatial frequencies.

We collected 324 trials per spatial frequency in each subject.

Perisaccadic detection experiment.

In a second control experiment, we tested the visibility of the perisaccadic probes used in the above experiment. Subjectively, the subjects did report to us that they consciously perceived the perisaccadic probes in the above experiment, despite the large magnitudes of mislocalization errors seen in RESULTS. Nonetheless, we still wanted to objectively confirm that the contrast used for the probe flashes was indeed high enough to avoid effects of saccadic suppression. We also wanted to confirm that, even if suppression was avoided by the high probe contrasts, perceptual visibility for such high-contrast probe flashes was still independent of the saccade target appearance. To do so, we collected full psychometric curves of probe detection (14). Thus, the experiment was the same as that described above, except that the probe flash now had variable contrast from trial to trial. Additionally, the probe flash time was either immediate upon online saccade detection, or at +11 or +35 ms. As we show in RESULTS, this timing allowed us to investigate probe visibility in the two mislocalization intervals in which we observed significant perisaccadic perceptual mislocalization in the main experiment above. Finally, in this task variant, the probe flash could appear at one of four cardinal locations relative to the saccade target center (and at an eccentricity halfway from the initial fixation position). The subjects' task was to report which of the four locations had a brief flash at it, and they did so via a response button box (indicating that the flash was to the right of, left of, above, or below the saccade target location). Note that the eccentricity of the probe flashes used here was roughly similar to the perceived eccentricities that we report in RESULTS for the mislocalization experiment, making the comparisons of the results in the two task variants meaningful.

Across trials, we varied the flash luminance to obtain full psychometric functions of flash detection sensitivity. The procedure was similar to that we described recently (14). Briefly, we performed a staircase procedure in the first session to obtain an initial estimate of perceptual threshold in a subject; in subsequent sessions, we also added additional

samples of flash contrast to sample more locations on the *x*-axis of the psychometric curves. As in the mislocalization experiment above, we also randomized the starting position of the whole stimulus display items across trials. That is, a constant random shift was applied to all stimulus positions in any given trial.

We collected 450–500 trials per spatial frequency in each subject.

Data Analysis

We detected saccades and microsaccades with our previously described methods (47, 50). Before analyzing any behavioral reports, we filtered the eye movement data to ensure matched saccade execution across low- and high-spatial frequency saccade targets. In the perisaccadic mislocalization task, we did so by binning the saccade landing points into bins of 0.5 × 0.5°. We also binned the saccade main sequence (51, 52) data points into bins of 0.5° × 40°/s. We then only accepted trials into the analyses that fulfilled the following criterion: they came from landing position and main sequence bins that had at least one trial repetition within them from each of the two saccade target image appearances (low and high spatial frequencies). This way, the saccades across image appearances were matched for both metrics and kinematics (see RESULTS). The typical numbers of trials per condition that remained after such filtering are like those described in the legend of Fig. 2.

In the perisaccadic detection task, we used a slightly different, but equally effective (see RESULTS), way of vector and kinematic matching. First, we defined a maximal radius (2°) for initial eye position at saccade triggering, and made sure that trials with both high- and low-spatial frequency saccade targets had the same initial starting position ranges. Similarly, we defined a maximal radius for final eye position at the end of the saccade, to make sure we had matched saccade vector ranges. Then, for each saccade direction (rightward or leftward), we ensured that the amplitudes and peak velocities of the saccades were matched regardless of whether the saccade target had a high or low spatial frequency (see RESULTS). We also excluded trials with saccadic reaction times < 80 ms or > 500 ms.

To analyze perisaccadic mislocalization, we first confirmed that we had matched saccade vectors as described above. We also confirmed that saccade peak velocities (that is, kinematics) were similar for low- and high-spatial frequency saccade targets (see RESULTS). We then recomputed all flash times relative to the actual saccade onset times after we properly detected the eye movements. After that, we collected each subject's click locations at different flash times. We classified the flash times into three categories (*t1*, *t2*, and *t3*) according to the histograms of flash times that we observed after recomputing the saccade onsets from the recorded eye movement data (see Fig. 1*B*). To summarize the subjects' click locations, we first remapped all data from leftward saccades to reflect their results across the vertical axis. That is, we flipped the horizontal axis for leftward saccades, in order to pool all results with the rightward saccades. Thus, in RESULTS we always show observations on a schematic vector representation having rightward saccades. After such remapping, we picked the median click location for each subject, each flash probe time, each flash probe location, and each saccade target appearance condition (low- or high-spatial frequency saccade target). Note that we always measured click locations relative to the stimulus locations; thus, the across-trial random shifts in global stimulus positions that we applied experimentally were removed in the analyses. To summarize the mislocalization effects, we measured for each trial the Euclidean distance from the actual flash location to the click location. In such summary analyses, we took (within a subject) the median Euclidean distances from all trials with forward flash positions; that is, for each subject we obtained a single (across trial) Euclidean distance measure across the three probe flash locations that were ahead of the saccade target. Larger mislocalization for a given condition (e.g., 1 saccade image appearance) was associated with a larger Euclidean distance. We then plotted the mean and SE of the distance across subjects, and we showed descriptive statistics and underlying individual subject results. We report all the statistical tests in RESULTS.

We also looked at the direction of the mislocalization vector for oblique probe flash positions. That is, mislocalization is known to have a two-dimensional landscape (along saccade direction and orthogonal to it) even if the saccades themselves are cardinal (16, 17). This two-dimensional landscape can be investigated by measuring the component of mislocalization independently either parallel to the saccade direction vector or orthogonal to it. Thus, we picked the two oblique flash positions that were ahead of the saccade target (at the ±45° diagonals) and that were expected to have the strongest oblique mislocalization (16, 17). Then, we compared how either their parallel or orthogonal mislocalization was different between the two image appearances of the saccade targets. For the parallel component we measured the horizontal component of their Euclidean distance measure described above, and for the orthogonal component we measured the vertical component.

We additionally compared mislocalization for flashes presented in the upper versus lower visual fields. That is, it is well established that the SC has an asymmetric representation of the upper and lower visual fields, which has been shown to play a potential role in the influence of saccade direction and visual field location on the strength of both perceptual mislocalization (17) and perceptual saccadic suppression (53). We therefore asked whether such an asymmetry could also differentially affect mislocalization strengths for upper and lower visual field flashes even with the same saccade direction. We did this by pooling data from both image conditions together (0.5 and 5 cycles/°) and analyzing mislocalization strength for either the oblique flash that was presented in the upper visual field or the one that was presented in the lower visual field. Very similar results were obtained when only inspecting the data individually for either the low- or high-spatial frequency saccade target conditions, so we decided to pool across spatial frequencies and maximize the numbers of trials that went into this analysis.

Finally, we correlated the end points of uninstructed saccades during cursor movement to the final reported locations with the mouse clicks. For each trial, we plotted the entire scanpath after the primary saccade of interest. This

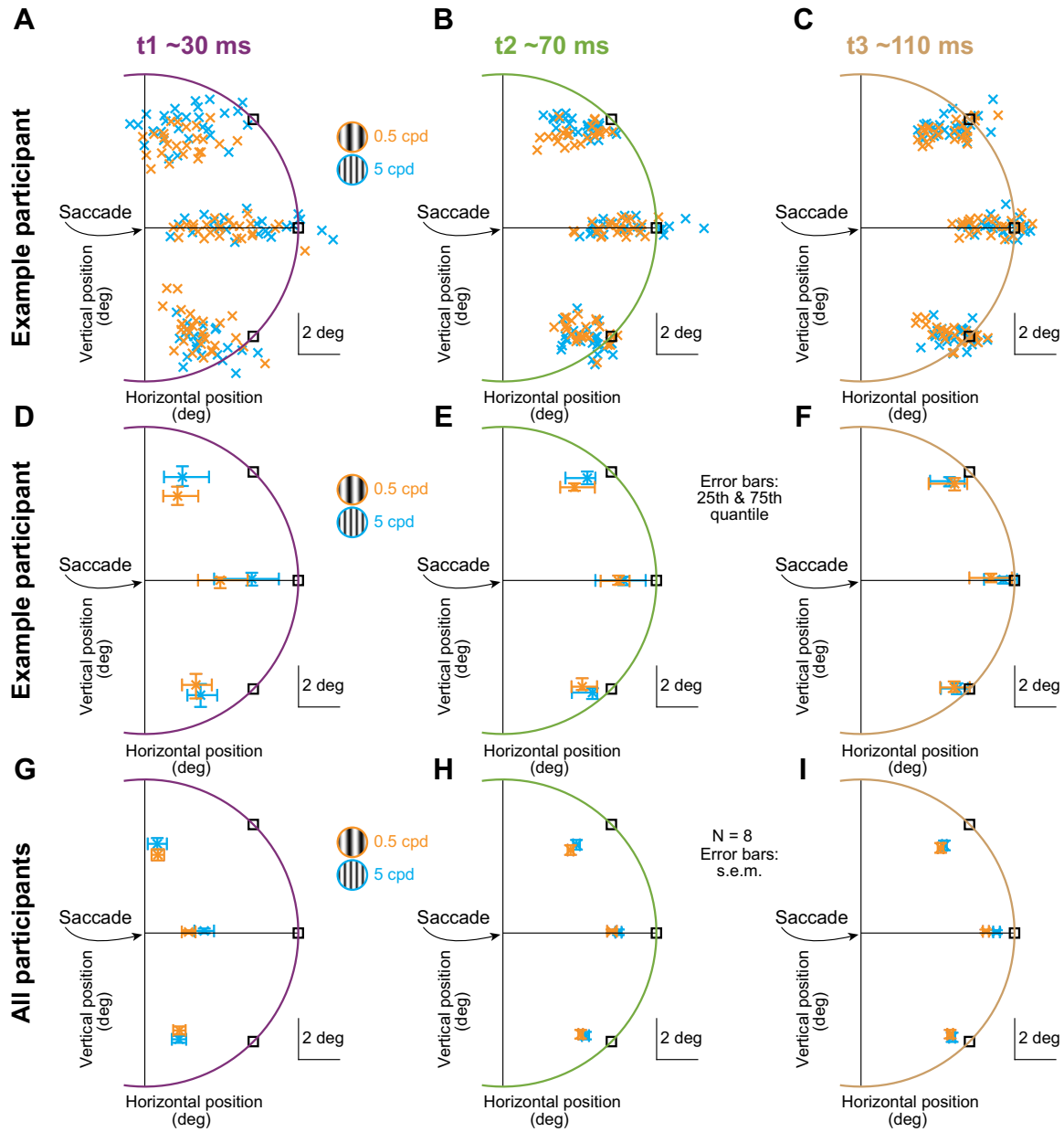

Figure 2. Stronger perisaccadic perceptual mislocalization with low-spatial frequency saccade targets. *A–C*: all click positions from 1 example subject (the same as in Fig. 1) after remapping all data to a rightward saccade direction (METHODS). The different panels show results from when the probe flashes were presented at *times t1* (*A*), *t2* (*B*), and *t3* (*C*), respectively, relative to saccade onset. Mislocalization got progressively weaker with time (compare the panels). Importantly, the mislocalization within a given time bin was different for the 2 different saccade target image appearances (compare the different colors in each panel). $N = 80, 73, 77$ trials for the clicks with the low-spatial frequency saccade target in *A*, *B*, and *C*, respectively. $N = 75, 77, 78$ trials for the clicks with the high-spatial frequency saccade target in *A*, *B*, and *C*, respectively. cpd, cycles/°. *D–F*: each symbol shows the median click location of the same subject for a given probe flash location, time, and saccade target image appearance. The range bars around each median click location indicate the interquartile extents of the data. *G–I*: for all analyses as in *D–F*, we averaged across 8 subjects. Error bars denote SE across the subjects. Also see Fig. 3 and Fig. 4 for more detailed quantitative analyses.

typically included a few saccades toward the final reported flash location (RESULTS). Then, we measured the final eye position at the time of the mouse cursor click, and we correlated this final eye position with the clicked location, both within individual subjects and across the population (and also across the different flash times).

All statistics on the perisaccadic mislocalization data were performed with MATLAB (version R2020b) and IBM SPSS Statistics (version 29.0).

In the perisaccadic detection experiment, we obtained psychometric curves of detection performance as a function of probe contrast level. To do that, we used the Psignifit 4

toolbox (54) for each subject individually, using a cumulative Gaussian function (and 0 lapse rate). We then averaged across the subjects' individual psychometric curves to obtain a population measure; thus, the population psychometric curve was the average of eight individual psychometric curves. We did this for each time bin of flash times relative to saccade onset (with the time bins defined as *t1a*, *t1b*, and *t2*, respectively; see RESULTS). Statistically, we performed bootstrapping to check whether perceptual detection depended on the saccade target image type. To do so, we created random permutations (10,000) in which we randomly picked trials for the two conditions (low- or high-spatial frequency saccade target) within each subject. When doing so, we kept the same numbers of observations per subject per condition, to maintain the sampling numbers consistent with our actual experimental data (especially after eye movement filtering). We then performed psychometric curve fits from such permuted data and measured the threshold at the 62.5% correct rate. Across the 10,000 permutations, we plotted the distributions of thresholds between the two sets of permuted conditions. If our actual measured threshold difference between low- and high-spatial frequency saccade targets was deviated by >95% of the threshold differences of the random permutations, then we deemed our measured threshold difference in the real experiment to be significant.

RESULTS

Our aim was to explore whether the strength of perisaccadic mislocalization could be modulated by the visual appearance of saccade targets, as might be predicted from observations of visual feature tuning in SC saccade-related motor bursts (39). To do so, we designed a psychophysical experiment in which humans reported the location of a brief perisaccadic probe flash that was presented at different times relative to saccade onset. Specifically, each trial consisted of an instruction to generate a primary saccade toward the center of a Gabor grating located near the center of the display screen (Fig. 1*A*). The initial fixation position was 8.5° to either the right or left of the grating center, thus requiring horizontal saccades. In addition, the Gabor grating could have one of two different spatial frequencies (METHODS). At different times relative to the online detection of a saccade (METHODS), we presented a brief, single-frame probe flash at one of four locations relative to the saccade target location. Three of these possible flashes were ahead of the saccade target, and one was behind it (Fig. 1*A*; METHODS). Note that, save for the saccade target image appearance manipulation, this task design was very similar to classic instantiations of the perisaccadic mislocalization paradigm (10, 11, 15, 16, 18), and also similar to our previous versions of it (17).

Figure 1*B* shows the distribution of probe flash times that we sampled for one example subject. During actual data collection, the computer triggered the probe flash at one of three possible delays after online saccade detection. However, the real delay was necessarily different, since online saccade detection required some data buffering for eye speed estimations (METHODS) and since there was some variance in the online speed estimates. Therefore, in post hoc analyses, we redetected all saccades (METHODS), and we then plotted the distributions of flash times in Fig. 1*B*. As can be seen, relative to the generated saccades (the gray region in Fig. 1*B* indicates the range of saccade end times observed for this subject, and Fig. 1, *C* and *D*, *bottom*, show radial eye speed from the same saccades), one set of times was intrasaccadic (labeled *t1*), another was around or shortly after saccade end (labeled *t2*), and the third was even longer after the saccades, when localization reports were expected to be nearer to the true probe flash locations on the display (labeled *t3*). Thus, our paradigm allowed us to analyze periods of significant perisaccadic mislocalization (*times t1* and *t2*) as well as periods closer to full recovery (*t3*). For simplicity, in what follows, we sometimes refer to *t1*, *t2*, and *t3* as 30 ms, 70 ms, and 110 ms, respectively.

Importantly, we ensured that the saccade vectors and kinematics were matched for the two different saccade target appearances. This was aided by having a small target spot in the middle of the gratings (39) (Fig. 1*A*), as well as by our filtering criteria described in METHODS. The net result was that the saccade distributions for the two different image types were virtually indistinguishable from each other between the low- and high-spatial frequency saccade targets (Fig. 1, *C* and *D*; 1 example subject's results are shown). Thus, we were now in a position to explore whether perisaccadic mislocalization was different for the two different saccade target images, despite the matched saccades.

Stronger Perisaccadic Mislocalization for Low-Spatial Frequency Saccade Targets

We analyzed each subject's click positions in each condition and time bin from Fig. 1. As stated in METHODS, we focused on the three probe flash locations ahead of the saccade target (1 directly along the saccade vector and 2 at ±45° oblique directions). This was the case especially because these three locations cause the strongest mislocalization (16, 17). Moreover, given that our saccades were significantly smaller than in previous studies of mislocalization (11, 16) [and were thus associated with smaller mislocalization strengths in general (17, 41)] and given the proximity of the probe opposite the saccade vector to the initial fixation position (METHODS), we felt that focusing only on the probe flash locations ahead of the saccade target was justified.

In Fig. 2, *A*–*C*, we show all click positions from one example subject's data. Each panel shows results from a given time bin, and this subject is the same subject whose eye movement data are shown in Fig. 1. As can be seen, the subject exhibited clear perisaccadic mislocalization, which diminished with increasing time from saccade onset. That is, regardless of which saccade target was visible (the 2 different colors in Fig. 2), the subject's click positions were closer to the saccade target in Fig. 2*A* than they were in Fig. 2, *B* and *C*. And, by *time t3* (110 ms), the click positions were closer to the true physical probe flash positions (Fig. 2*C*) (with the existence of some expected residual systematic undershoot biases; Refs. 48, 49). This fact, that the reported positions were more accurate for later flash times, confirms our intuition that the click errors seen in Fig. 2, *A* and *B*, were not due to distortions in the subject's memory of the flash position; if they were, then there was no reason for these errors to decrease for the later flash times, since the trial lengths after flash onsets were generally all very similar across conditions.

Indeed, in our previous work, we found very minimal impacts of long memory delays on (saccade free) memory-based reporting of stimulus locations with a mouse cursor (48, 49).

Importantly, Fig. 2, *A–C*, show that the subject's behavioral reports clearly depended on the appearance of the saccade target. This is seen through the different conditions in Fig. 2, *A–C*. In orange we show the clicks with the low-spatial frequency saccade target, and in blue we show clicks with the high-spatial frequency saccade target. There was stronger mislocalization, especially for the oblique probe flash positions, with the low-spatial frequency saccade target. This was also evident in the median click positions for the different probe flash locations and times (Fig. 2, *D–F*; error bars denote interquartile ranges). Thus, in this example subject, perisaccadic mislocalization depended on the visual appearance of the saccade target, even with metrically and kinematically matched saccades.

These results were consistent across our eight subjects. We repeated the analyses of Fig. 2, *D–F*, for each subject, and we then plotted the mean and SE values across the subjects in Fig. 2, *G–I*. There were systematic differences between the two different saccade target image appearances, which we investigated further in Fig. 3. Specifically, we computed, for each trial, the Euclidean distance between the physical location of the probe and the individual click position. Then, within each subject, we took the median distance across all three flash locations ahead of the saccade target location, and we did this separately for the different probe flash times. The saturated data points in Fig. 3 show the mean and SE across eight subjects, and the gray data points show individual subject results. Note that the *y*-axis ranges in Fig. 3, *A–C*, are not the same across the three panels, and this is because mislocalization got progressively smaller with increasing delay between the saccade and probe onsets (Fig. 2); we wanted to zoom into the data ranges of each panel individually. As can be seen, for each of *times t1* and *t2*, all but one subject showed a stronger perisaccadic mislocalization for the low-spatial frequency saccade target than for the high-spatial frequency saccade target (Fig. 3, *A* and *B*). At *time t3*, all but two subjects still showed this effect, although the overall mislocalization strength was much weaker given the longer time after the saccade (Fig. 2). Again, the weaker mislocalization with later flash times after the saccade rules out an interpretation of our results as being solely due to distortions in working memory.

We further quantified these effects by plotting in Fig. 3*D* the difference in the mislocalization strength between the low- and high-spatial frequency saccade target images as a function of probe flash time. This difference was similar for *times t1* and *t2*, and it was clearly positive at each of these two time points (with only 1 outlier subject in each case). Statistically, we performed a repeated-measures two-way ANOVA with the factors time and spatial frequency of the saccade target. Both main effects were significant [time: $F(2,14) = 67.78$, $P < 10^{-7}$, $\eta^2 = 0.906$; spatial frequency of the saccade target: $F(1,7) = 69.04$, $P < 10^{-4}$, $\eta^2 = 0.908$]. There was no significant interaction between these two factors. This is consistent with the observation that the difference in mislocalization strength for the two different saccade target image appearances was very similar for *times t1* and *t2* in Fig. 3*D*. We also performed post hoc tests (with Bonferroni correction), which revealed a significant difference in mislocalization strength between the saccade target image types for both *time t1* ($P = 0.015$) and *time t2* ($P = 0.025$). These results suggest that a perisaccadic phenomenon, which can potentially depend on

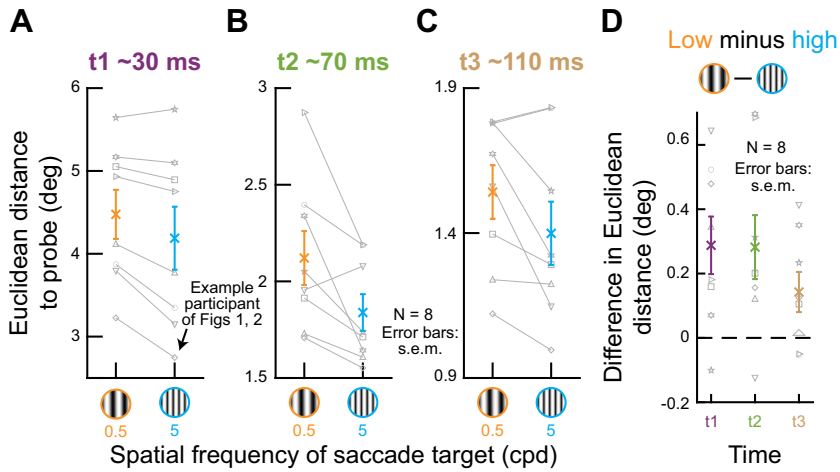

Figure 3. Population summaries of the results in Fig. 2. *A*: the saturated data points show the mean and SE across subjects ($N = 8$) of the Euclidean distances between the median click location at *time t1* and the true probe flash location (for the 3 probes ahead of the saccade target; Fig. 2). The gray data points show individual subject results. All but 1 subject had stronger perisaccadic perceptual mislocalization for the low-spatial frequency saccade target. The data with the diamond symbol in this and subsequent figures correspond to the same example subject of Fig. 1 and Fig. 2. *B*: similar results for *time t2*. Again, all but 1 subject had stronger perisaccadic perceptual mislocalization for the low-spatial frequency saccade target. *C*: similar results for *time t3*. Here, all but 2 subjects showed stronger mislocalization for the low-spatial frequency saccade target. Note that the *y*-axes are different in the different panels because of the time-varying amplitude of the mislocalization effect (Fig. 2). cpd, cycles/°. *D*: at each flash time (*x*-axis values), we plotted the difference in mislocalization strength between the low- and high-spatial frequency saccade target image trials. A positive difference indicates stronger mislocalization for the low-spatial frequency saccade target. The saturated data points show the mean and SE across subjects, and the gray data points show the individual subject results. Especially at *times t1* and *t2* (with strong perceptual mislocalization), there was stronger mislocalization for the low-spatial frequency saccade target appearance. Also see Fig. 4.

ascending SC projections (28–30, 32), depends on the visual appearance of the saccade target (especially at *times t1* and *t2*). This implies that visual feature tuning in SC neuronal movement commands (39) may, in turn, potentially provide more than just the vector information of executed movements via SC-sourced corollary discharge signals.

Stronger Orthogonal Mislocalization for Low-Spatial Frequency Saccade Targets

In the analyses of Fig. 2, we additionally noticed that oblique probe flash positions exhibited a stronger dependence of mislocalization strength on saccade target image appearance in the direction orthogonal to the saccade vector than in the direction parallel to it. Specifically, at *time t1*, with maximal mislocalization strengths in our experiments, both the example subject (Fig. 2, *A* and *D*) and the population (Fig. 2*G*) showed a bigger deviation in the vector direction between the true probe flash position and the behavioral reports of the subjects, suggesting a difference in the orthogonal component of mislocalization. Such a difference was masked by the analyses of Fig. 3, which pooled different probe flash positions and which were somewhat agnostic of the two-dimensional nature of perisaccadic mislocalization. Therefore, to explore this further, we expressed the mislocalization effect according to its two spatial components: one along the direction of the saccade (parallel to it) and one orthogonal to the saccade vector (Fig. 4*A*). We then compared the mislocalization effect in each direction separately for the two different saccade target image appearances.

We first compared the mislocalization effects along the saccade direction (Fig. 4, *B–E*), which is generally the direction in which mislocalization is strongest even for oblique flash positions (16, 17). Although the trends were all the same as those seen in Fig. 3, the clearest statistical effect now emerged only at *time t2*. Specifically, we performed a repeated-measures two-way ANOVA with the factors time and spatial frequency of the saccade target. Both main effects were significant [time: $F(2,14) = 47.27$, $P < 10^{-6}$, $\eta^2 = 0.871$; spatial frequency of the saccade target: $F(1,7) = 6.6$, $P = 0.037$, $\eta^2 = 0.486$], and there was no interaction. However, in post hoc tests (with Bonferroni correction), there was only a significant difference for the two types of saccade target at *time t2* (Fig. 4, *C* and *E*). Thus, this might indicate that the saccade target image appearance effects seen in Fig. 3, especially at maximal mislocalization periods (*time t1*), might have been dominated by the orthogonal component of mislocalization. We confirmed this to be the case. We performed the same tests but now on mislocalization orthogonal to the saccade direction (Fig. 4, *F–I*). Again both main effects were significant [time: $F(2,14) = 4.34$, $P = 0.034$, $\eta^2 = 0.383$; spatial frequency of the saccade target: $F(1,7) = 11.12$, $P = 0.013$, $\eta^2 = 0.614$]. On top of that, there was also an interaction between the factors time and spatial frequency of the saccade target [$F(2,14) = 9.47$, $P = 0.003$, $\eta^2 = 0.575$], indicating that the difference in mislocalization for the different

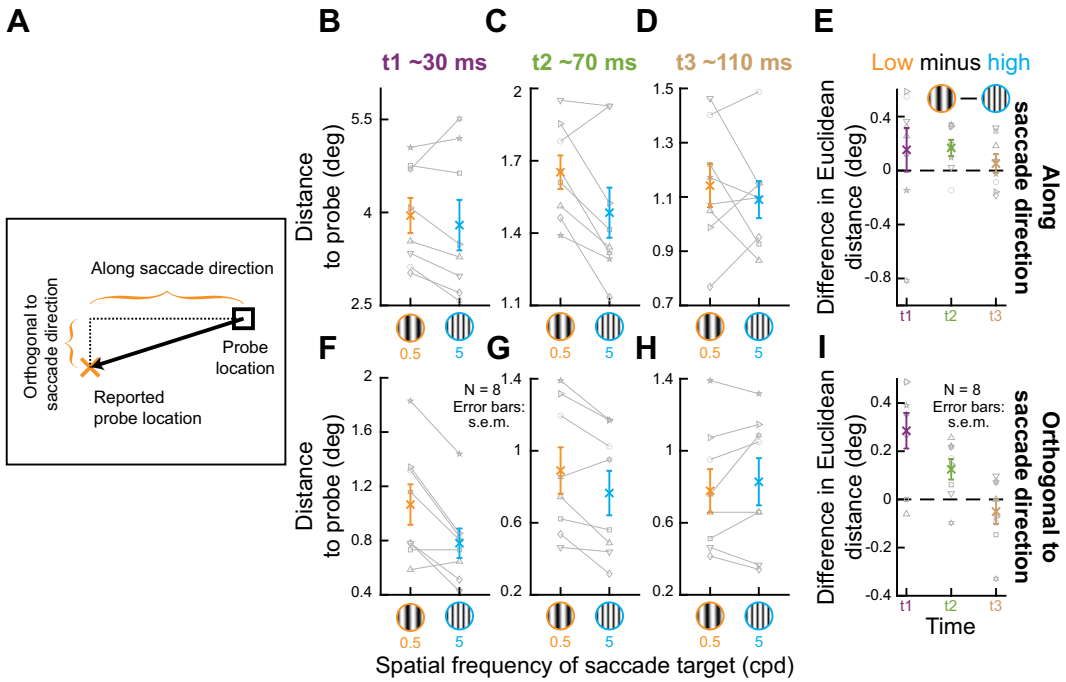

Figure 4. Stronger orthogonal mislocalization with low-spatial frequency saccade targets. *A*: our analysis approach for assessing the strength of orthogonal mislocalization. For the oblique probe flash positions ahead of the saccade target, we measured the 2 components of mislocalization separately. One component was along the saccade direction (measuring the horizontal distance between the reported and true probe locations), and one component was orthogonal to the saccade direction (measuring the distance between true and reported probe locations along the orthogonal axis). *B–E*: same as Fig. 3, *A–D*, but for the parallel component of mislocalization. The trends were all the same as in Fig. 3. but the significant effect of saccade target image appearance only emerged at *time t2* (see text). This might suggest that orthogonal mislocalization might have dominated the effects of Fig. 3. especially at *time t1*. *F–I*: we confirmed this by repeating the same analyses, but this time for the orthogonal component of mislocalization. Note how there was clearly stronger orthogonal mislocalization for low- than high-spatial frequency saccade targets, especially at *time t1*. All other conventions in this figure are the same as those in Fig. 3. cpd, cycles/°.

saccade targets differed as a function of time. Consistent with this, a post hoc test (with Bonferroni correction) revealed that the significant difference as a function of saccade target image appearance was present at both *times t1* ($P = 0.006$) and *t2* ($P = 0.022$) (Fig. 4*I*). Thus, even the two-dimensional landscape of perisaccadic mislocalization (16, 17) depends on the saccade target image appearance, and this effect was clearest at *time t1* (Fig. 4*I*).

Stronger Mislocalization for Probes in the Upper Rather than Lower Visual Field

The SC is known for its asymmetric representation of the upper and lower visual fields (22, 23). Therefore, we also wondered whether, even for purely horizontal saccades, mislocalization strength could additionally depend on the visual field locations of the probe flashes. For example, it could be the case that upper visual field magnification in the SC (22) is an additional topographic map distortion that can potentially modify mislocalization patterns. Testing this possibility would provide even further motivation for the idea of a putative involvement of the SC in remapping mechanisms that can cause perisaccadic mislocalization. Moreover, if validated, showing different perisaccadic mislocalization for the upper and lower visual fields would add to increasing evidence that perisaccadic vision in general might follow SC visual field asymmetries rather than asymmetries in performance that occur in the absence of saccades (likely cortically mediated), which are of exactly opposite sign to the SC asymmetries (55–58). Indeed, this is already known to be the case for perisaccadic suppression of visual sensitivity (53). Other human evidence includes perisaccadic visual meridian effects (59), visual field asymmetries in crowding and saccadic precision (60), and visual motion processing in the brain (for example, while walking) (61).

Combining all trials from both the low- and high-spatial frequency saccade targets, we compared mislocalization strength when the probe was presented in either the upper or lower visual field. That is, we explored the two oblique probe locations ahead of the saccade target location, which were perfectly symmetric with respect to the saccade vector, except for the visual field difference (METHODS). The results are shown in Fig. 5, which is formatted similarly to Fig. 3 and Fig. 4. However, here, instead of comparing the effects of the saccade target image appearance on mislocalization, we now compared probe flash locations. As can be seen, there was clearly stronger mislocalization in the upper, rather than lower, visual field. We tested this statistically with a repeated-measures two-way ANOVA (factors: time and probe location). The test results were significant for both the factors of time [$F(2,14) = 62.58$, $P < 10^{-6}$, $\eta^2 = 0.899$] and probe location [$F(1,7) = 23.22$, $P = 0.002$, $\eta^2 = 0.768$]. There was also a significant interaction between these two factors [$F(2,14) = 6.46$, $P = 0.01$, $\eta^2 = 0.48$) (Fig. 5*D*). Moreover, post hoc tests revealed that the difference between upper and lower visual field probe locations was significant at all three tested times (*t1*: $P = 0.001$; *t2*: $P = 0.005$; *t3*: $P = 0.014$) (Fig. 5*D*). Therefore, there was a clear dependence of perisaccadic mislocalization strength on visual field location, even with purely horizontal saccades. Note that we reached similar conclusions when we performed these analyses individually for either the low- or high-spatial frequency saccade targets as well (this can also be easily inferred from Fig. 2).

Thus, our results so far indicate that perisaccadic mislocalization depends on both saccade target image appearance (Figs. 2–4) and retinotopic probe flash location (Fig. 5). We next related these effects to unin-structed eye movements during the response phase of our experimental trials, and we then confirmed that our mislocalization observations were not explained by an altered visibility of the probe flashes by the visual conditions of our experiments.

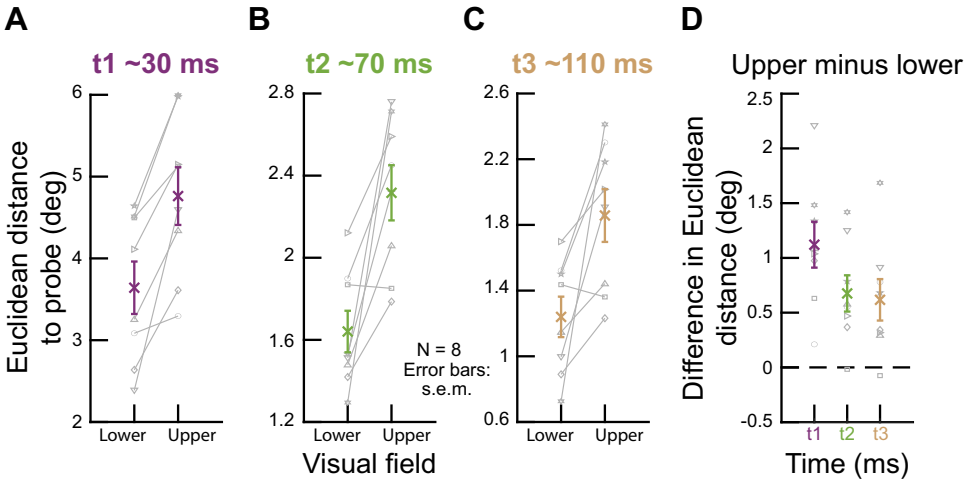

Figure 5. Stronger perisaccadic perceptual mislocalization for probe flashes in the upper, rather than lower, visual field. This figure is formatted identically to Fig. 3 except that the comparison is now between visual field locations rather than saccade target image appearances. Specifically, we now combined all trials, whether the spatial frequency of the saccade target grating was 0.5 or 5 cycles/°. Then, we considered the mislocalization strength of the 2 probe locations that were in oblique directions relative to the saccade target. Because of the configuration of our display, these 2 probe locations were at identical positions relative to the saccade target (METHODS). However, one of them was in the upper visual field, and the other was in the lower visual field. As can be seen, there was stronger mislocalization for upper visual field probes. All other conventions are identical to those in Fig. 3. *A*, *B*, and *C*: results for *times t1*, *t2*, and *t3*, respectively. *D*: difference between upper and lower visual fields.

J Neurophysiol • doi:10.1152/jn.00368.2024 • www.jn.org

Similar Mislocalization Effects by Analyzing Uninstructed Saccades While Subjects Responded

In our mislocalization paradigm, we did not provide any instructions to our subjects on what to do with their eyes while reporting their perceived flash locations via mouse cursor clicks (METHODS). Nonetheless, we consistently observed that the subjects automatically generated secondary saccades pointing almost exactly to where they clicked (Fig. 6*A* shows such example trials from one of our subjects). This prompted us to ask whether the eye movement end point locations at the time of mouse cursor clicks correlated with the mouse cursor click positions that we had asked for. This was most definitely the case. For example, for the same subject as in Fig. 6*A*, Fig. 6*B* plots the Euclidean distance between the mouse cursor click location and the true flash location on the *x*-axis, and the figure simultaneously plots, on the *y*-axis, the Euclidean distance between the same subject's eye position (measured −50 to 0 ms relative to mouse cursor click time) and the true flash location. The two measures were highly correlated (Pearson's $r = 0.92$; $P < 10^{-12}$; including all trials from the subject with all possible probe flash times and also pooling across spatial frequencies of the saccade target). This was also true across all of our subjects, as shown in Fig. 6*C*. In this figure, each subject is represented by three symbols covering the three possible flash times. As can be seen, there was clear correlation between mouse cursor reports and uninstructed eye position reports (Pearson's $r = 0.98$; $P < 10^{-17}$ across all shown data points). Therefore, in perisaccadic mislocalization paradigms (for example, in monkeys), it is possible to use secondary eye movements after the primary saccade of interest to objectively measure mislocalization effects (see DISCUSSION).

Similar Flash Visibility for Low- and High-Spatial Frequency Saccade Targets

In the above experiment and analyses, we were confident that the probe flashes were suprathreshold (and thus highly visible to the subjects) because of their high contrast (METHODS). Therefore, we interpreted the results as suggesting that mislocalization can indeed depend on the visual appearance of the saccade target (Figs. 1–4). However, it could still be the case that the appearance of the saccade target (especially given that it was a relatively big image patch) could, in one way or another, cause different detectability levels of the brief perisaccadic probe flashes. Therefore, in a second experiment, we explicitly characterized the detectability of the flashes at different contrast levels. This allowed us to confirm that the detectability of the high-contrast probe flashes in the results above was the same for either the low- or high-spatial frequency saccade targets.

We perisaccadically flashed brief, low-contrast probes (METHODS), and we measured contrast sensitivity curves. The paradigm itself was very similar to that used above. However, instead of localizing probe flashes, the subjects knew in advance that the probe could appear at one of the four cardinal directions around the saccade target (Fig. 7*A*; METHODS). They simply had to report which of the four locations displayed the flash.

As in the mislocalization experiment, we also had variable probe flash times relative to saccade onset. Specifically, Fig. 7*B* shows the timing of the probe flashes in this new experiment. As can be seen, the trigger points of the probe flashes after online saccade detection (METHODS) resulted in a bimodal distribution of flash times. The second mode (at

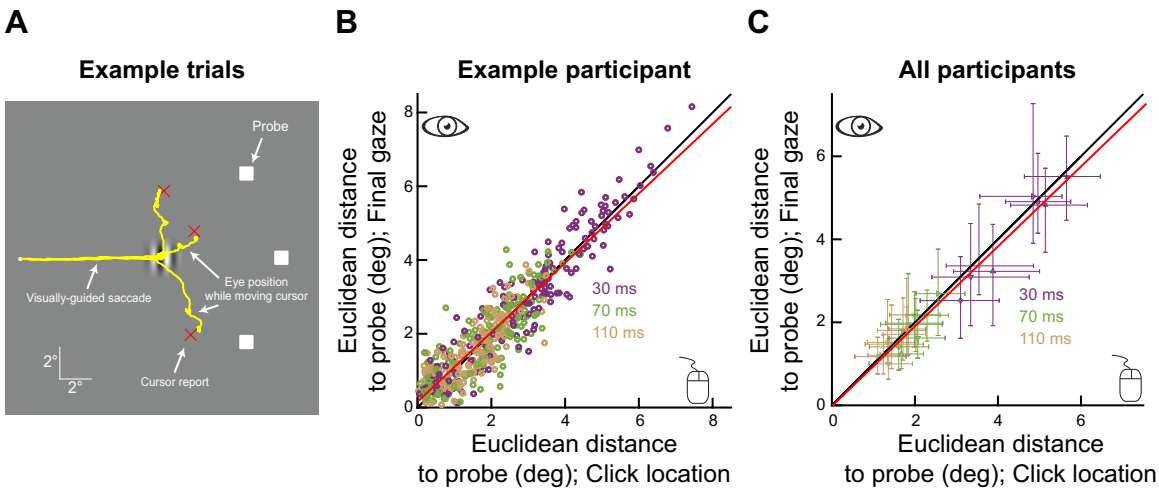

Figure 6. Uncovering of perisaccadic perceptual mislocalization via uninstructed eye movements during the reporting phase of our experimental trials. *A*: 3 example trials from 1 subject (different from that of Fig. 1 and Fig. 2), showing eye movement behavior and the corresponding cursor click locations for a probe flash presented at *time t1* in our perisaccadic mislocalization experiment. The primary, visually guided saccade was from the left to the right, and it is this saccade that was paired with a brief probe flash. When it was time to report the perceived flash location, there were uninstructed saccades by the subject while moving the cursor. The first of these saccades in each trial clearly reflected the mislocalization effect because it was very different from a veridical saccade to the true flash location (indicated by the white squares); the subject then typically made 1 or 2 more smaller saccades and fixations, to fine-tune the final report. In the end, eye position was very close to the final report (red cross) on each trial. Thus, uninstructed eye movements during the final reporting phase of our trials reflected the perisaccadic mislocalization effect. *B*: for the same subject, we measured the Euclidean distance of final eye position at the time of the cursor click to the true probe flash location. We then plotted this measure against the Euclidean distance of the cursor click location itself to the true probe flash location. There was a very high correlation across all trials (black is the unity slope line, and red is the regression line). *C*: median Euclidean distances of each subject for each flash probe time (each subject's data are represented by 3 distinct points for the 3 tested flash times). Error bars denote the 25th to 75th quantiles, and the red line is the regression fit to the data.

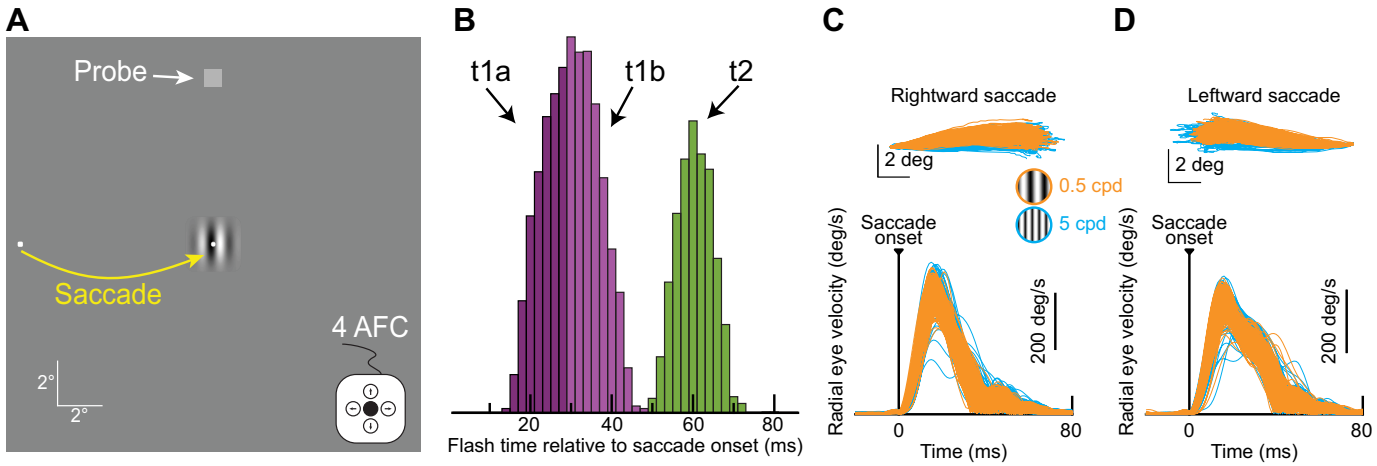

Figure 7. Probing perisaccadic perceptual detectability with different saccade target image appearances. *A*: subjects generated a rightward (shown) or leftward saccade toward the center of a low- or high-spatial frequency grating. At different times relative to online saccade detection, we presented a very brief probe flash at 1 of 4 cardinal positions (pure up shown). Subjects had to indicate at which 1 of the 4 locations they detected the stimulus [4-alternative forced choice (4 AFC) task]. *B*: distribution of flash times relative to saccade onset in our data from a sample subject (different from the ones of Figs. 1, 2, and 6). We classified flash times according to the 3 seen categorizations, and we labeled the categories *t1a*, *t1b*, and *t2*, respectively. *t2* was quantitatively similar to *t2* in the perceptual mislocalization experiment above. *C* and *D*: analyses similar to Fig. 1, *C* and *D*, demonstrating that we matched saccades in terms of both their metrics and kinematics across the 2 saccade target image appearances. cpd, cycles/°.

~70 ms; Fig. 7*B*) was very similar to that in *t2* of the original experiment. Since *time t2* in that experiment was still a time in which we had clear differential mislocalization performance for the two different saccade target image appearances (Figs. 2–5), this time bin in the current experiment was ideal to check whether the detectability of the probe flashes was any different for the two different saccade target image features. We thus labeled this second mode in Fig. 7*B* as *t2*, since it was quantitatively similar to *time t2* in the original experiment. As for the first mode in the histogram of Fig. 7*A*, we split it into two subcategories (*t1a* and *t1b*) because we wanted to check for a worst-case scenario about potential visibility differences with maximal saccadic suppression, which would be expected for *t1a* (the closest time to saccade onset).

In the current experiment, we also matched the saccade metrics and kinematics across the two different image appearances of the saccade target, just like we did in the perisaccadic mislocalization experiment above. For example, Fig. 7, *C* and *D*, show eye movement analyses very similar to those in Fig. 1, *C* and *D*, from a sample subject. As can be seen, the saccade properties were well matched across the two different image appearances of the saccade target. Therefore, we could now check the psychometric curves.

Even under the worst-case scenario of maximal saccadic suppression, perceptual detection reached ceiling performance at probe luminances well below those that we used in the perisaccadic mislocalization experiment described above. This can be seen from Fig. 8. In Fig. 8*A*, we show the psychometric curves of performance from one example subject (the same one as in Fig. 7, *C* and *D*). One pair of curves is for probe flashes occurring at *time t1a* from Fig. 7*B*, and another pair is for probe flashes occurring at *time t2*. In each pair, one curve is for the low-spatial frequency saccade target, and the other is for the high-spatial frequency saccade target. For reference, the probe contrast used in the perisaccadic mislocalization experiment above was at an *x*-axis value of 70 in these psychometric curves. Thus, in all cases, this subject's performance reached ceiling performance for much lower probe contrasts, even at the worst-case scenario of near-maximal saccadic suppression. Importantly, at *time t2*, when mislocalization still showed significant differential effects between saccade target appearances (Figs. 2–4), the full psychometric curves in this current experiment were completely overlapping (and with very low detection thresholds). Thus, the results of Figs. 2–4 cannot be explained by different probe detectability due to the different saccade target image appearances used in the experiments.

These results were consistent across all eight subjects (Fig. 8*B*). Interestingly, at the population level, we found a small, but significant ($P < 0.05$; bootstrapping; METHODS) difference in the semisaturation contrasts of the two saccade target image appearances only at *time t1a* (but not at *times t1b* and *t2*). This might suggest that even perisaccadic suppression itself, which can putatively also rely on corollary discharge information (28, 62), might also depend on the saccade target visual features. This is consistent with both the predictions of the neurophysiology (39) and the general motivations for the present study. Nonetheless, from the perspective of perisaccadic mislocalization, which is the main topic of the present study, the most important feature of the results of Fig. 8*B* is that, at the probe contrasts used in Figs. 1–5 (*x*-axis luminance of 70 in Fig. 8*B*), perceptual detectability of the probe flashes was clearly at ceiling and did not depend on the saccade target image appearance. Thus, the results of Figs. 2–4 cannot be explained by visual-visual interactions caused by the different image appearances of the low- and high-spatial frequency saccade target gratings.

Therefore, our observations, combined, suggest that perisaccadic mislocalization seems to depend on the visual appearance of the saccade target (Figs. 1–4) and that this dependence is not explained by a simple visual interaction

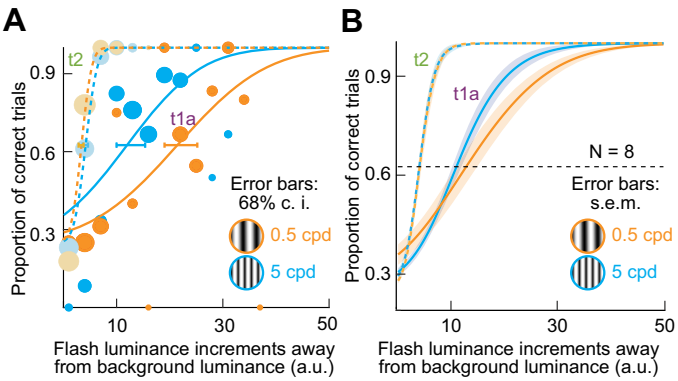

Figure 8. Dependence of probe detection on the saccade target image appearance, but only for very low-contrast probes and only during maximal saccadic suppression. *A*: psychometric curves of perceptual detection performance from 1 example subject (same as that of Fig. 7). Since this was a 4-alternative forced choice task, chance performance was at a 25% correctness rate, and threshold was defined as the contrast giving rise to a 62.5% correctness rate. When the probe appeared during *time t1a* in Fig. 7*B*. the subject showed a higher detection threshold for the low-spatial frequency saccade target than for the high-spatial frequency saccade target. However, note that ceiling performance was reached by luminance index 50 above background. For reference, the probe luminance in Figs. 1–5 was at 70 on the *x*-axis. Thus, even at *time t1a*, the probe in Figs. 1–5 was highly detectable. For *time t2*, the thresholds were much lower, and the psychometric curves were almost completely overlapping. Note that at this time perceptual mislocalization still significantly differentiated between the saccade target image appearances (Figs. 2–4), suggesting that such differentiation was not mediated by different probe visibility for the 2 different types of saccade targets that we used. Error bars denote 68% confidence interval (c.i.). The size of each shown data point is scaled by the numbers of observations. a.u., Arbitrary units. *B*: population results. Each curve shows the average of the 8 subjects' psychometric curves, and error bars denote SE. At *time t1a*, there was a small threshold difference between the different saccade target appearances ($P < 0.05$; bootstrapping; METHODS). However, at *t2* (and *t1b*; not shown), there were no differences. Importantly, performance was clearly at ceiling at the probe contrasts used in the mislocalization experiment. Thus, the results of Figs. 2–5 cannot be explained by altered detectability of the probe flashes by the different saccade target image appearances.

between such appearance and the ability to detect high-contrast perisaccadic probe flashes (Fig. 7 and Fig. 8).

DISCUSSION

In this study, we were motivated by our recent observations that SC motor bursts can be different for different visual appearances of the saccade target, even with matched saccade metrics and kinematics (39). Such difference suggests that the motor bursts in the SC might be dissociated from the exact moment-to-moment execution of the eye movements (23, 63). Assuming that such visual sensory tuning in SC motor bursts underlies a function, we hypothesize that it is used via the ascending projections from the SC to other brain areas. Such projections may be thought of as corollary discharge (24, 31, 32, 64): neurons on the SC map that are active at the time of saccade onset indicate the vector of the intended saccade (65), and such vector information (and the concomitant time-locked onset of the bursts) could help to either suppress visual sensitivity (29, 66) or remap retinotopic response fields (32) in the cortex. Given that the SC integrates a large amount of visual information from many brain areas, including from the retina (67), visual information in the SC motor bursts at the time of saccades could allow the predictive processes associated with corollary discharge (29, 32, 38, 68) to be more general than just informing cortex of the timing and vector of saccades. These processes could additionally enable transsaccadic feature prediction to anticipate the foveated image appearance after the saccade. In other words, visual information in the SC at the time of saccade onset could be relayed for postsaccadic visual processing in the fovea. Although this idea needs to be explicitly tested neurophysiologically (for example, by investigating the transfer of visual information to foveal neurons in the SC and elsewhere across saccades), our goal here was to check whether perceptual correlates of it could potentially be observed. Thus, the scope of our present contribution is solely the documentation of a new type of phenomenology that is associated with perisaccadic mislocalization.

We specifically found that the properties of perisaccadic mislocalization depended on the appearance of the saccade target. Moreover, this effect was not explained by different visibility of the perisaccadic high-contrast probe flashes as a function of the saccade target appearance. We believe that these results motivate revisiting earlier neurophysiological investigations of corollary discharge from the SC (25, 26, 29, 31, 64, 66), but now from the perspective of saccades to images. For example, one could start mapping neurons in the pulvinar or medio-dorsal thalamus, which are involved in corollary discharge signaling from the SC to the cortex, but specifically during active vision tasks involving saccades to images rather than to spots. This could clarify if and how these brain areas may relay information about the visual appearance of saccade targets to their recipient neurons. It could also help explain what other roles these relay areas might have. For example, if SC visual responses, and not just saccade-related motor bursts, are relayed (25), then what is the purpose of such relaying, and what are the feature tuning properties of visual responses in areas like the pulvinar and the medio-dorsal thalamus?

These and related questions can also help identify the potential ecological benefits of having stronger perisaccadic mislocalization for low-spatial frequency saccade targets, as we found here. Of course, in general, we believe that it would be quite rare to experience perisaccadic mislocalization in real life, since it is unlikely that brief visual stimuli will suddenly appear right around the time of a saccade. However, and as mentioned above, the key to perisaccadic mislocalization is that the mechanisms revealed by such a laboratory phenomenon will still be relevant in everyday life. We speculate that certain aspects of visual processing in the brain must (and do) emphasize the processing of low spatial frequencies in the incoming retinal images, particularly given the known spectral content of natural scenes (69, 70). For example, saccades in both humans and monkeys have consistently faster reaction times for low-spatial frequency targets (71–73), and SC visual responses are consistently stronger and earlier for low-spatial frequency images (73). Thus, it could be that an alteration of transsaccadic processing for low-spatial frequency saccade targets, as revealed by stronger perisaccadic mislocalization, enables a targeted highlighting, both pre- and postsaccadically, of such important images.

Although we did not focus on perisaccadic suppression too much in our present study, our second experiment already allowed us to additionally measure perceptual suppression at *time t1a* (Fig. 7 and Fig. 8). Interestingly, both the sample subject (Fig. 8*A*) and the population of subjects (Fig. 8*B*) showed that there was potentially stronger suppression (higher thresholds in the psychometric curves) when the saccade target had a low spatial frequency than when it had a high spatial frequency. This might suggest that even saccadic suppression strength, and not just perisaccadic mislocalization, can depend on the visual appearance of the saccade targets. In addition to being consistent with our hypotheses above about corollary discharge incorporating saccade target appearance in its signal, this is also consistent with our observations on perisaccadic mislocalization in our main experiment. Indeed, we previously measured perceptual saccadic suppression in humans, with saccades across different visual textures, and we again observed stronger perisaccadic suppression with low-spatial frequency textures (14). Although our interpretations in that earlier study focused on the visual components of perisaccadic suppression, results from the present study and the sensory-tuned SC motor bursts (39) hint that motor-related components could also potentially account for at least some of these differences. Nonetheless, what is clear from our present detection experiments is that they cannot fully explain the mislocalization ones. This is because the probe contrasts in the mislocalization experiments were very high compared to when there could be any potential image dependencies of detection performance. In fact, at *time t2*, the detection psychometric curves were completely overlapping for the two different saccade target image appearances (and almost fully recovered relative to *time t1a*), but the mislocalization strength was still different.

Having said that, the saccade target in our experiment (and not just the representations of the probe flashes) was swept on the retina across saccades. As a result, there was a retinal motion sweep, which could potentially contribute to our observed results. In other words, if the motion sweep had different properties for the two different saccade target images, then it could still be possible that visual-visual interactions could account for our observations of different mislocalization strengths across the image types. However, by deliberate experimental design choice, our gratings were orthogonal to the saccade vector direction. Thus, there was maximal retinal blurring of these gratings by the saccades. So, it seems less likely that this could have fully explained our mislocalization results. Moreover, we always placed a small fixation spot (over a gray background) right in the middle of each grating (39), which further allowed us to control for the postsaccadic fixation statistics across trials (and independently of the spatial frequency of the saccade target). Also, our detectability experiments suggested that the probe contrast was so much above threshold contrast, especially at *time t2*, as to be affected by potential subtle differences in the retinal motion sweeps associated with low- and high-spatial frequency grating saccade targets. Finally, perisaccadic mislocalization can still occur with saccades toward a blank (74).

More generally, we believe that our experiments motivate the study of visual perception from an active perspective. In addition, taking a more ecological approach to active vision than with simple dot stimuli would be useful. It can reveal visual-visual and visual-motor interactions that are most relevant for natural behavior. More importantly, such an ecological perspective should also consider the state of the body itself, and not just the environmental context (63). Indeed, maintaining proper bodily posture and orientation requires a sustained tonic activation of eye and neck muscles, and proprioception of the neck muscles can have a significant impact on aligning a pointing response with a visual target impinging on the retina (63). Taking such an approach can merge fields of vision, oculomotor control, body posture, and reference frames in a most interesting manner.

In our case, our segue into an ecological approach was driven by our interest in visual field asymmetries. For example, it is believed that overrepresentation of the upper visual field by the SC (22) could be ecologically relevant for active orienting across species (67, 75). Intriguingly, this motivated us to explore the effects of upper and lower visual field flashes in terms of mislocalization strength (Fig. 5), and we indeed found stronger perisaccadic mislocalization in the upper visual field. This is reminiscent of a differential effect also in saccadic suppression strength between the upper and lower visual fields (53), and it would be interesting in the future to further merge the topics of visual field asymmetries and perisaccadic vision but from a much more neurophysiological perspective.

In that regard, we have already utilized our observations in Fig. 6 to port our visual mislocalization paradigms to the monkey animal model (for further neurophysiology) (76). Specifically, the results of Fig. 6 provided us with very useful information because they suggest that one could train monkeys to report their perceived flash location with a secondary eye movement after the primary one. This opens the door for advanced neurophysiological experiments, including with causal perturbation manipulations, using identical behavioral paradigms to humans. This is an enticing opportunity.

DATA AVAILABILITY

Data will be made available upon reasonable request.

GRANTS

We were funded by the Deutsche Forschungsgemeinschaft (DFG; German Research Foundation) through the SFB 1233 Robust Vision (project number: 276693517). We were also funded by the DFG through the SPP 2205 Evolutionary Optimization of Neuronal Processing (project number: HA 6749/3-2) and the SPP 2411 Sensing LOOPS: Cortico-subcortical Interactions for Adaptive Sensing (project number: HA 6749/11-1).

DISCLOSURES

No conflicts of interest, financial or otherwise, are declared by the authors.

AUTHOR CONTRIBUTIONS

M.P.B., A.F.D., and Z.M.H. conceived and designed research; performed experiments; analyzed data; interpreted results of experiments; prepared figures; drafted manuscript; edited and revised manuscript; and approved final version of manuscript.

REFERENCES

1. **Bridgeman B**, **Hendry D**, **Stark L.** Failure to detect displacement of the visual world during saccadic eye movements. *Vision Res* 15: 719–722, 1975. doi:10.1016/0042-6989(75)90290-4.
2. **Bridgeman B**, **van der Heijden AH**, **Velichkovsky BM.** A theory of visual stability across saccadic eye movements. *Behav Brain Sci* 17: 247–258, 1994. doi:10.1017/S0140525X00034361.
3. **Schweitzer R**, **Rolfs M.** Intra-saccadic motion streaks as cues to linking object locations across saccades. *J Vis* 20: 17, 2020. doi:10.1167/jov.20.4.17.
4. **Rolfs M**, **Schweitzer R.** Coupling perception to action through incidental sensory consequences of motor behaviour. *Nat Rev Psychol* 1: 112–123, 2022. doi:10.1038/s44159-021-00015-x.
5. **Honda H.** Perceptual localization of visual stimuli flashed during saccades. *Percept Psychophys* 45: 162–174, 1989. doi:10.3758/bf03208051.
6. **Dassonville P**, **Schlag J**, **Schlag-Rey M.** Oculomotor localization relies on a damped representation of saccadic eye displacement in human and nonhuman primates. *Vis Neurosci* 9: 261–269, 1992. doi:10.1017/s0952523800010671.
7. **Latour PL.** Visual threshold during eye movements. *Vision Res* 2: 261–262, 1962. doi:10.1016/0042-6989(62)90031-7.
8. **Zuber BL**, **Stark L.** Saccadic suppression: elevation of visual threshold associated with saccadic eye movements. *Exp Neurol* 16: 65–79, 1966. doi:10.1016/0014-4886(66)90087-2.
9. **Beeler GW Jr.** Visual threshold changes resulting from spontaneous saccadic eye movements. *Vision Res* 7: 769–775, 1967. doi:10.1016/0042-6989(67)90039-9.
10. **Cai RH**, **Pouget A**, **Schlag-Rey M**, **Schlag J.** Perceived geometrical relationships affected by eye-movement signals. *Nature* 386: 601–604, 1997. doi:10.1038/386601a0.
11. **Ross J**, **Morrone MC**, **Burr DC.** Compression of visual space before saccades. *Nature* 386: 598–601, 1997. doi:10.1038/386598a0.
12. **Hafed ZM**, **Krauzlis RJ.** Microsaccadic suppression of visual bursts in the primate superior colliculus. *J Neurosci* 30: 9542–9547, 2010. doi:10.1523/JNEUROSCI.1137-10.2010.
13. **Chen CY**, **Hafed ZM.** A neural locus for spatial-frequency specific saccadic suppression in visual-motor neurons of the primate superior colliculus. *J Neurophysiol* 117: 1657–1673, 2017. doi:10.1152/jn.00911.2016.
14. **Idrees S**, **Baumann MP**, **Franke F**, **Münch TA**, **Hafed ZM.** Perceptual saccadic suppression starts in the retina. *Nat Commun* 11: 1977, 2020. doi:10.1038/s41467-020-15890-w.
15. **Lappe M**, **Awater H**, **Krekelberg B.** Postsaccadic visual references generate presaccadic compression of space. *Nature* 403: 892–895, 2000. doi:10.1038/35002588.
16. **Kaiser M**, **Lappe M.** Perisaccadic mislocalization orthogonal to saccade direction. *Neuron* 41: 293–300, 2004. doi:10.1016/s0896-6273(03)00849-3.
17. **Grujic N**, **Brehm N**, **Gloge C**, **Zhuo W**, **Hafed ZM.** Perisaccadic perceptual mislocalization is different for upward saccades. *J Neurophysiol* 120: 3198–3216, 2018. doi:10.1152/jn.00350.2018.
18. **Klingenhoefer S**, **Krekelberg B.** Perisaccadic visual perception. *J Vis* 17: 16, 2017. doi:10.1167/17.9.16.
19. **Ostendorf F**, **Fischer C**, **Gaymard B**, **Ploner CJ.** Perisaccadic mislocalization without saccadic eye movements. *Neuroscience* 137: 737–745, 2006. doi:10.1016/j.neuroscience.2005.09.032.
20. **VanRullen R.** A simple translation in cortical log-coordinates may account for the pattern of saccadic localization errors. *Biol Cybern* 91: 131–137, 2004. doi:10.1007/s00422-004-0514-2.
21. **Chen CY**, **Hoffmann KP**, **Distler C**, **Hafed ZM.** The foveal visual representation of the primate superior colliculus. *Curr Biol* 29: 2109–2119.e7, 2019. doi:10.1016/j.cub.2019.05.040.
22. **Hafed ZM**, **Chen CY.** Sharper, stronger, faster upper visual field representation in primate superior colliculus. *Curr Biol* 26: 1647–1658, 2016. doi:10.1016/j.cub.2016.04.059.
23. **Zhang T**, **Malevich T**, **Baumann MP**, **Hafed ZM.** Superior colliculus saccade motor bursts do not dictate movement kinematics. *Commun Biol* 5: 1222, 2022. doi:10.1038/s42003-022-04203-0.
24. **Sommer MA**, **Wurtz RH.** A pathway in primate brain for internal monitoring of movements. *Science* 296: 1480–1482, 2002. doi:10.1126/science.1069590.
25. **Sommer MA**, **Wurtz RH.** What the brain stem tells the frontal cortex. I. Oculomotor signals sent from superior colliculus to frontal eye field via mediodorsal thalamus. *J Neurophysiol* 91: 1381–1402, 2004. doi:10.1152/jn.00738.2003.
26. **Sommer MA**, **Wurtz RH.** What the brain stem tells the frontal cortex. II. Role of the SC-MD-FEF pathway in corollary discharge. *J Neurophysiol* 91: 1403–1423, 2004. doi:10.1152/jn.00740.2003.
27. **Sommer MA**, **Wurtz RH.** Brain circuits for the internal monitoring of movements. *Annu Rev Neurosci* 31: 317–338, 2008. doi:10.1146/annurev.neuro.31.060407.125627.
28. **Berman RA**, **Joiner WM**, **Cavanaugh J**, **Wurtz RH.** Modulation of presaccadic activity in the frontal eye field by the superior colliculus. *J Neurophysiol* 101: 2934–2942, 2009. doi:10.1152/jn.00053.2009.
29. **Berman RA**, **Cavanaugh J**, **McAlonan K**, **Wurtz RH.** A circuit for saccadic suppression in the primate brain. *J Neurophysiol* 117: 1720–1735, 2017. doi:10.1152/jn.00679.2016.
30. **Shin S**, **Sommer MA.** Division of labor in frontal eye field neurons during presaccadic remapping of visual receptive fields. *J Neurophysiol* 108: 2144–2159, 2012. doi:10.1152/jn.00204.2012.
31. **Guthrie BL**, **Porter JD**, **Sparks DL.** Corollary discharge provides accurate eye position information to the oculomotor system. *Science* 221: 1193–1195, 1983. doi:10.1126/science.6612334.
32. **Sommer MA**, **Wurtz RH.** Influence of the thalamus on spatial visual processing in frontal cortex. *Nature* 444: 374–377, 2006. doi:10.1038/nature05279.
33. **Zirnsak M**, **Steinmetz NA**, **Noudoost B**, **Xu KZ**, **Moore T.** Visual space is compressed in prefrontal cortex before eye movements. *Nature* 507: 504–507, 2014. doi:10.1038/nature13149.
34. **Zirnsak M**, **Moore T.** Saccades and shifting receptive fields: anticipating consequences or selecting targets? *Trends Cogn Sci* 18: 621–628, 2014. doi:10.1016/j.tics.2014.10.002.
35. **Hartmann TS**, **Zirnsak M**, **Marquis M**, **Hamker FH**, **Moore T.** Two types of receptive field dynamics in area V4 at the time of eye movements? *Front Syst Neurosci* 11: 13, 2017. doi:10.3389/fnsys.2017.00013.
36. **Neupane S**, **Guitton D**, **Pack CC.** Dissociation of forward and convergent remapping in primate visual cortex. *Curr Biol* 26: R491–R492, 2016. doi:10.1016/j.cub.2016.04.050.
37. **Neupane S**, **Guitton D**, **Pack CC.** Two distinct types of remapping in primate cortical area V4. *Nat Commun* 7: 10402, 2016. doi:10.1038/ncomms10402.
38. **Wang X**, **Fung CC**, **Guan S**, **Wu S**, **Goldberg ME**, **Zhang M.** Perisaccadic receptive field expansion in the lateral intraparietal area. *Neuron* 90: 400–409, 2016. doi:10.1016/j.neuron.2016.02.035.
39. **Baumann MP**, **Bogadhi AR**, **Denninger AF**, **Hafed ZM.** Sensory tuning in neuronal movement commands. *Proc Natl Acad Sci USA* 120: e2305759120, 2023. doi:10.1073/pnas.2305759120.
40. **Baumann MP**, **Idrees S**, **Münch TA**, **Hafed ZM.** Dependence of perceptual saccadic suppression on peri-saccadic image flow properties and luminance contrast polarity. *J Vis* 21: 15, 2021. doi:10.1167/jov.21.5.15.
41. **Hafed ZM.** Alteration of visual perception prior to microsaccades. *Neuron* 77: 775–786, 2013. doi:10.1016/j.neuron.2012.12.014.
42. **Brainard DH.** The Psychophysics Toolbox. *Spat Vis* 10: 433–436, 1997.
43. **Kleiner M**, **Brainard D**, **Pelli DG.** What's new in Psychtoolbox-3? (Abstract). *Perception* 36, 2007.
44. **Pelli DG.** The VideoToolbox software for visual psychophysics: transforming numbers into movies. *Spat Vis* 10: 437–442, 1997.
45. **Cornelissen FW**, **Peters EM**, **Palmer J.** The Eyelink Toolbox: eye tracking with MATLAB and the Psychophysics Toolbox. *Behav Res Methods Instrum Comput* 34: 613–617, 2002. doi:10.3758/bf03195489.
46. **Greilich J**, **Baumann MP**, **Hafed ZM.** Microsaccadic suppression of peripheral perceptual detection performance as a function of foveated visual image appearance. *J Vis* 24: 3, 2024. doi:10.1167/jov.24.11.3.
47. **Chen CY**, **Hafed ZM.** Postmicrosaccadic enhancement of slow eye movements. *J Neurosci* 33: 5375–5386, 2013. doi:10.1523/JNEUROSCI.3703-12.2013.
48. **Willeke KF**, **Tian X**, **Buonocore A**, **Bellet J**, **Ramirez-Cardenas A**, **Hafed ZM.** Memory-guided microsaccades. *Nat Commun* 10: 3710, 2019. doi:10.1038/s41467-019-11711-x.

49. **Willeke KF**, **Cardenas AR**, **Bellet J**, **Hafed ZM.** Severe distortion in the representation of foveal visual image locations in short-term memory. *Proc Natl Acad Sci USA* 119: e2121860119, 2022. doi:10.1073/pnas.2121860119.
50. **Bellet ME**, **Bellet J**, **Nienborg H**, **Hafed ZM**, **Berens P.** Human-level saccade detection performance using deep neural networks. *J Neurophysiol* 121: 646–661, 2019. doi:10.1152/jn.00601.2018.
51. **Bahill AT**, **Clark MR**, **Stark L.** The main sequence, a tool for studying human eye movements. *Math Biosci* 24: 191–204, 1975. doi:10.1016/0025-5564(75)90075-9.
52. **Zuber BL**, **Stark L**, **Cook G.** Microsaccades and the velocity-amplitude relationship for saccadic eye movements. *Science* 150: 1459–1460, 1965. doi:10.1126/science.150.3702.1459.
53. **Fracasso A**, **Buonocore A**, **Hafed ZM.** Peri-saccadic orientation identification performance and visual neural sensitivity are higher in the upper visual field. *J Neurosci* 43: 6884–6897, 2023. doi:10.1523/JNEUROSCI.1740-22.2023.
54. **Schütt HH**, **Harmeling S**, **Macke JH**, **Wichmann FA.** Painfree and accurate Bayesian estimation of psychometric functions for (potentially) overdispersed data. *Vision Res* 122: 105–123, 2016. doi:10.1016/j.visres.2016.02.002.
55. **Barbot A**, **Xue S**, **Carrasco M.** Asymmetries in visual acuity around the visual field. *J Vis* 21: 2, 2021. doi:10.1167/jov.21.1.2.
56. **Montaser-Kouhsari L**, **Carrasco M.** Perceptual asymmetries are preserved in short-term memory tasks. *Atten Percept Psychophys* 71: 1782–1792, 2009. doi:10.3758/APP.71.8.1782.
57. **He S**, **Cavanagh P**, **Intriligator J.** Attentional resolution and the locus of visual awareness. *Nature* 383: 334–337, 1996. doi:10.1038/383334a0.
58. **Rubin N**, **Nakayama K**, **Shapley R.** Enhanced perception of illusory contours in the lower versus upper visual hemifields. *Science* 271: 651–653, 1996. doi:10.1126/science.271.5249.651.
59. **Liu X**, **Melcher D**, **Carrasco M**, **Hanning NM.** Presaccadic preview shapes postsaccadic processing more where perception is poor. *Proc Natl Acad Sci USA* 121: e2411293121, 2024. doi:10.1073/pnas.2411293121.
60. **Greenwood JA**, **Szinte M**, **Sayim B**, **Cavanagh P.** Variations in crowding, saccadic precision, and spatial localization reveal the shared topology of spatial vision. *Proc Natl Acad Sci USA* 114: E3573–E3582, 2017. doi:10.1073/pnas.1615504114.
61. **Gilaie-Dotan S.** Visual motion serves but is not under the purview of the dorsal pathway. *Neuropsychologia* 89: 378–392, 2016. doi:10.1016/j.neuropsychologia.2016.07.018.
62. **Diamond MR**, **Ross J**, **Morrone MC.** Extraretinal control of saccadic suppression. *J Neurosci* 20: 3449–3455, 2000. doi:10.1523/JNEUROSCI.20-09-03449.2000.
63. **Goffart L.** Cerebralization of mathematical quantities and physical features in neural science: a critical evaluation. *Eur Phys J Web Conf* 300: 01007, 2024. doi:10.1051/epjconf/202430001007.
64. **Sparks DL**, **Porter JD.** Spatial localization of saccade targets. II. Activity of superior colliculus neurons preceding compensatory saccades. *J Neurophysiol* 49: 64–74, 1983. doi:10.1152/jn.1983.49.1.64.
65. **Lee C**, **Rohrer WH**, **Sparks DL.** Population coding of saccadic eye movements by neurons in the superior colliculus. *Nature* 332: 357–360, 1988. doi:10.1038/332357a0.
66. **Berman RA**, **Wurtz RH.** Signals conveyed in the pulvinar pathway from superior colliculus to cortical area MT. *J Neurosci* 31: 373–384, 2011. doi:10.1523/JNEUROSCI.4738-10.2011.
67. **Hafed ZM**, **Hoffmann KP**, **Chen CY**, **Bogadhi AR.** Visual functions of the primate superior colliculus. *Annu Rev Vis Sci* 9: 361–383, 2023. doi:10.1146/annurev-vision-111022-123817.
68. **Duhamel JR**, **Colby CL**, **Goldberg ME.** The updating of the representation of visual space in parietal cortex by intended eye movements. *Science* 255: 90–92, 1992. doi:10.1126/science.1553535.
69. **Ruderman DL**, **Bialek W.** Statistics of natural images: scaling in the woods. *Phys Rev Lett* 73: 814–817, 1994. doi:10.1103/PhysRevLett.73.814.
70. **Tolhurst DJ**, **Tadmor Y**, **Chao T.** Amplitude spectra of natural images. *Ophthalmic Physiol Opt* 12: 229–232, 1992. doi:10.1111/j.1475-1313.1992.tb00296.x.
71. **White BJ**, **Stritzke M**, **Gegenfurtner KR.** Saccadic facilitation in natural backgrounds. *Curr Biol* 18: 124–128, 2008. doi:10.1016/j.cub.2007.12.027.
72. **Ludwig CJ**, **Gilchrist ID**, **McSorley E.** The influence of spatial frequency and contrast on saccade latencies. *Vision Res* 44: 2597–2604, 2004. doi:10.1016/j.visres.2004.05.022.
73. **Chen CY**, **Sonnenberg L**, **Weller S**, **Witschel T**, **Hafed ZM.** Spatial frequency sensitivity in macaque midbrain. *Nat Commun* 9: 2852, 2018. doi:10.1038/s41467-018-05302-5.
74. **Zimmermann E**, **Morrone MC**, **Burr DC.** The visual component to saccadic compression. *J Vis* 14: 13, 2014. doi:10.1167/14.12.13.
75. **Previc FH.** Functional specialization in the lower and upper visual-fields in humans - its ecological origins and neurophysiological implications. *Behav Brain Sci* 13: 519–542, 1990. doi:10.1017/S0140525X00080018.
76. **Baumann MP, Hafed ZM.** Two-dimensional perisaccadic visual mislocalization in rhesus macaque monkeys (Preprint). *bioRxiv*, 2024. doi:10.1101/2024.11.20.624548.